Saudi Pharmaceutical Journal 26 (2018) 876–885

Contents lists available at ScienceDirect

Saudi Pharmaceutical Journal

journal homepage: www.sciencedirect.com

Original article

Resveratrol-loaded PLGA nanoparticles mediated programmed cell death in prostate cancer cells

Anmar M. Nassir [a], Naiyer Shahzad [b,*], Ibrahim A.A. Ibrahim [b], Iqbal Ahmad [c,d,*], Shadab Md [e], Mohammad R. Ain [f]

[a] Department of Surgery, Faculty of Medicine, Umm Al-Qura University, Makkah, Saudi Arabia
[b] Department of Pharmacology and Toxicology, Faculty of Medicine, Umm Al-Qura University, Makkah, Saudi Arabia
[c] Nanomedicine Research Lab., Department of Pharmaceutics, School of Pharmaceutical Education and Research, Jamia Hamdard, New Delhi, India
[d] Advance Nanomeds, NSEZ, Noida, Uttar Pradesh, India
[e] Department of Pharmaceutical Technology, School of Pharmacy, International Medical University, Jalil Perkasa, Kuala Lumpur, Malaysia
[f] Department of Clinical Pharmacy, College of Pharmacy, Prince Sattam Bin Abdulaziz University, Alkharj, Saudi Arabia

ARTICLE INFO

Article history:
Received 28 December 2017
Accepted 14 March 2018
Available online 15 March 2018

Keywords:
Resveratrol
PLGA nanoparticles
Prostate cancer
LNCaP cells
Apoptosis
Drug delivery

ABSTRACT

Resveratrol (RL), a natural polyphenol, is known for its diverse biological effects against various human cancer cell lines. But low aqueous solubility, poor bioavailability, and stability limit its efficacy against prostate cancer. In this study polymeric nanoparticles encapsulating resveratrol (RLPLGA) were designed and their cytotoxic and mode of apoptotic cells death against prostate cancer cell line (LNCaP) was determined. Nanoparticles were prepared by solvent displacement method and characterized for particle size, TEM, entrapment efficiency, DSC and drug release study. RLPLGA exhibited a significant decrease in cell viability with 50% and 90% inhibitory concentration (IC_{50} and IC_{90}) of 15.6 ± 1.49 and 41.1 ± 2.19 μM respectively against the LNCaP cells. This effect was mediated by apoptosis as confirmed by cell cycle arrest at G1-S transition phase, externalization of phosphatidylserine, DNA nicking, loss of mitochondrial membrane potential and reactive oxygen species generation in LNCaP cells. Furthermore, significantly greater cytotoxicity to LNCaP cells was observed with nanoparticles as compared to that of free RL at all tested concentrations. RLPLGA nanoparticles presented no adverse cytotoxic effects on murine macrophages even at 200 μM. Our findings support the potential use of developed resveratrol loaded nanoparticle for the prostate cancer chemoprevention/ chemotherapy with no adverse effect on normal cells.

1. Introduction

Resveratrol (RL), a naturally occurring polyphenol possesses many medicinal properties including anti-inflammatory, anti-aging, cardiovascular, antiviral, anti-oxidant, and neuroprotective effects (Richard et al., 2011). RL regulates several molecular signal transduction pathways that lead to inhibition or death of cancer cells (She et al., 2001). The inhibitory effect of resveratrol on MDA-MB-231 breast cancer cells (Pozo-Guisado et al., 2002), pancreatic cancer cell lines PANC-1 and AsPC-1 and colon cancer cell line (Caco-2) (Ding and Adrian, 2002) are already reported. Hsieh and Wu exhibited its inhibitory effect on the G1-S cell cycle transition in PC-3, DU-145 as well as LNCaP cells thereby increasing apoptosis. Also, RL caused a reduction in both intracellular and secreted prostate-specific antigen in LNCaP prostate cells without affecting the androgen receptor expression (Hsieh and Wu, 1999). RL acts through various mitogen-activated protein kinases (MAPK) and protein kinase C (PK-C) mediated pathways to induce apoptosis in both DU145 and LNCaP cells (Shih et al., 2004). RL also facilitates the reduction in oxidative stress and decreasing the production of nitric oxide within premalignant PC-3 and DU-145 cells, that inhibits the growth and spread of prostate cancer (PCa) (Ratan et al., 2002). The pronounced chemo-preventive effect of RL on PCa is also supported by *in vivo* studies (Seeni et al., 2008; Wang et al., 2008). Some clinical studies also presented the beneficial effects of

* Corresponding authors at: Department of Pharmacology and Toxicology, Faculty of Medicine, Umm Al-Qura University, P.O. Box 7182, Makkah 21955, Saudi Arabia (N. Shahzad), Advance Nanomeds, Plot No. 142/20A, NSEZ, Noida 201305, Uttar Pradesh, India (I. Ahmad).
E-mail addresses: shahzadnaiyer@gmail.com (N. Shahzad), iqbal_ahmad2@yahoo.co.in (I. Ahmad).
Peer review under responsibility of King Saud University.

Production and hosting by Elsevier

https://doi.org/10.1016/j.jsps.2018.03.009
1319-0164/

resveratrol in cancer management. For example, 39 patients, randomized, double-blind, placebo-controlled clinical trial performed on breast cancer subjects for 3 months showed a decrease in RASSF-1α methylation with 5 or 50 mg twice daily dose resveratrol (Zhu et al., 2012). Likewise, in colorectal cancer patients (20 subjects), 500 or 1000 mg of resveratrol was given 8 days prior to surgery. Ki-67 staining showed a significant reduction in tumor cell proliferation (Patel et al., 2010). The effect of resveratrol in prostate cancer patients was studied in two independent trials, of which one showed a beneficial effect (increase in PSADT) (Paller et al., 2015), while other study showed no positive effect (Kjær et al., 2015). The possible reason for the inefficient therapeutic utilization of RL can be attributed to its poor aqueous solubility (3 mg/100 mL) and rapid metabolism mediated low bioavailability (Ahmad et al., 2016; Singh et al., 2016). Walle et al. reported that even if it shows a high oral absorption in human, the systemic bioavailability is quite low. At 6 h after the oral dose of 25 mg, the mean plasma concentration of only 290 ± 68 ng/ml (1.3 μM) was seen after which there was exponential decrease (Walle et al., 2004). So, the basic rationale of this study lies in the fact that the encapsulation of natural bioactive into a nanocarrier provides numerous advantages in terms of protection against biological degradation, improved oral absorption and, bioavailability as well as increased intracellular penetration (Jabir et al., 2012). Many studies have utilized the potential of nanocarrier-based drug delivery systems to direct antiproliferative agents against prostate cancer, which include, but not limited to, liposomes (Narayanan et al., 2009), nanoemulsion (Anuchapreeda et al., 2011), magnetic nanoparticles (Johannsen et al., 2010), drug aptamer-gold nanoparticle conjugate (Kim et al., 2010) and various other polymeric and lipid nanoparticles (Sanna and Sechi, 2012). Among the polymeric system, submicron polylactic-co-glycolic acid (PLGA) nanoparticles have been tried by many groups both for passive and active targeting of therapeutic agents against prostate cancers (Hsieh and Wu, 1999). Guo and co-workers developed bovine serum albumin-based nanoparticles for the encapsulation of RL which significantly repressed the growth rate of human primary ovarian carcinoma cells that were subcutaneously implanted in nude mice (Guo et al., 2010). Likewise, Narayanan et al. developed RL and Curcumin co-encapsulated liposomes which significantly increased levels of the drug in serum and prostate as well as improved cell growth inhibition and induction of apoptosis as well as decreased prostatic adenocarcinoma. So, this study aims to show the activity of RL loaded PLGA nanoparticles on cancer chemoprevention of LNCaP cell line. A comparative assessment of RLPLGA nanoparticles with the plain drug in terms of cell growth inhibitions and analysis of apoptosis is presented in this study. Finally, cytotoxicity on murine macrophages by MTT cell proliferation assay was assessed to determine the safety profile.

2. Materials and methods

Reagents

Resveratrol ≥ 99% (HPLC) was purchased from Sigma-Aldrich, USA. Annexin V-FITC and the Apo-Direct kits were purchased from Roche Inc., Basel, Switzerland. Fetal bovine serum (FBS) was procured from Gibco-BRL. Terminal Deoxynucleotidyl Transferase Biotin-dUTPNick End Labeling (TUNEL) assay kit, Limulus amebocyte lysate (LAL) kit, and caspase-3 assay kit were purchased from Thermo Fisher Scientific, USA. Other chemicals and solvents used were of analytical grade and used without further purification.

2.1. RP-HPLC method for resveratrol quantification

The RP-HPLC method was adopted from Cvetković et al. (2015). Briefly, HPLC-3000 system (Analytical Technologies Ltd., India) consisting of binary pump, UV–Visible detector, column oven, and a manual injector system (20 μL) was used to cross-validate the method. The data analyses of the method was performed on CXTH-3000 software. An isocratic RP-HPLC technique was employed in which methanol was used as mobile phase (flow rate 1 mL/min), injection volume was 20 μL and a detection wavelength was set at 306 nm. The separation was carried out at 35 °C using ACE® 5 C18 column (250 mm × 4.6 mm, 5 μm) (Advanced Chromatography Technologies Ltd, Scotland).

2.2. Cell culture

LNCaP cells were obtained from the American Type Culture Collection (ATCC) and grown in RPMI 1640 medium at 37 °C (pH 7.4) supplemented with 10% fetal bovine serum (FBS), penicillin (100 IU mL^{-1}) and streptomycin (100 μg mL^{-1}) in a humidified atmosphere of 5% CO_2 and sub-cultured in fresh RPMI-1640 medium at an average density 2×10^5 cells mL^{-1}.

2.3. Preparation of resveratrol-loaded nanoparticles

RL loaded PLGA nanoparticles were developed by nanoprecipitation technique. PLGA and RL4:1, 2:1 and 1:1 (w/w) (total weigh t = 50 mg) were vortexed in 2 mL of acetone for complete solubilization. The prepared solution was added dropwise using a glass syringe to 10 mL of PVA solution having a concentration of 2.5 mg/mL, 5 mg/mL, and 7.5 mg/mL. The mixture was magnetically stirred for 5 h complete evaporation of acetone. The dispersion was centrifuged at 45,000g for 25 min at 10 °C at re-dispersed in water three times for nanoparticle separation (Hermle Labor Technik, Germany). The nanoparticles were lyophilized using mannitol (5% w/w) as the cryoprotectant. The process was optimized by performing 9 runs of 3^2-factorial design with ratios of PLGA/RL (Factor A) and concentration of PVA solution (Factor B) as independent variables. The particles size and entrapment efficiency were, studied for each run. Placebo nanoparticles were prepared in the same way except that the drug was not added.

2.4. Characterization of nanoparticles

2.4.1. Particle size analysis

The particle size and particle size distribution were determined by Zetasizer Nano ZS (Malvern Instrument, Worcestershire, UK). 20 mg of lyophilized nanoparticle was dispersed in 1 mL of water, which was further diluted to 50 mL and analyzed in disposable zeta sizer cuvette.

2.4.2. Transmission electron microscopy

Morphology as well as the particle size of the nanoparticles were analyzed by transmission electron microscopy (TEM). A drop of nanoparticle dispersion in water was placed over a holey grid and air-dried and analyzed under the electron microscope (JEOL 2100F, JEOL USA, INC). 100 particles from each quadrant were measured for particle size and a size vs number histogram was plotted to get the particle size distribution.

2.4.3. Entrapment efficiency (%EE)

Entrapment efficiency was determined by dissolving the 20 mg dried nanoparticles in 1 mL acetone followed by centrifugation. The supernatant acetone was analyzed for RL by HPLC. The percent ratio of drug added initially to the amount present in the nanoparticle gives entrapment efficiency.

2.4.4. Differential scanning calorimetry

Differential scanning calorimetry was performed for RL and RLPLGA using a DSC instrument (Perkin Elmer, USA).

2.4.5. In vitro drug release study

The drug release study was performed in phosphate buffer saline (PBS) pH 7.4 using dialysis bag method as described previously in the literature (Singh et al., 2013).

2.5. MTT assay

For MTT [3-(4,5-dimethylthiazol-2-yl)-2,5-diphenyltetrazolium bromide] assay, LNCaP Cells were seeded in the flat bottom 96-well plate (5 x 10^4 in 200 μL culture medium per well) and incubated for 48 h at 37 °C with 5% CO_2. They were treated with the native drug (RL) or RLPLGA nanoparticles (suspended in water) and incubated for 48 h at concentrations of 10, 20, 30, 40, 50 and 100 μM equivalent of RL concentrations. 5 mg/mL MTT was freshly prepared in PBS and filtered through 0.2 μm syringe filter. To each well, 2 mL of MTT solution was added and the plate was incubated for 4 h at 37 °C in a humidified 5% CO_2. Consequently, the media were removed and 2 mL of DMSO was added to each well to solubilize the formazan. The optical densities were measured at 570 nm for each well. The percentage of cell viability was evaluated as the percentage ratio of optical density of the treated wells to that of untreated wells.

2.6. Analysis of phosphatidylserine (PS) externalization

Double staining with Annexin-V/PI (propidium iodide) of LNCaP cells were performed for PS exposure analysis. Briefly, the cells were incubated with RL and RLPLGA nanoparticles at various concentrations (0–50 μM) for 24 h. Untreated as well as treated cells were centrifuged for 10 min at 3000 ×*g*. The pellets were washed twice in cold PBS, re-suspended in 100 μL Annexin V-FLUOS labeling solution and incubated for 15 min in the dark at 26 °C. 400 μL of incubation buffer was then added, mixed and observed using a BD LSR II flow cytometer and analyzed using Deva software (Sheth et al., 2012).

2.7. TUNEL assay

DNA fragmentation was determined by the TdT (Terminal deoxynucleotidyl transferase) mediated Nick end labeling method. Firstly, the treated cells were washed with PBS and fixed with 4% paraformaldehyde on ice for 1 h. Subsequently, cells were washed with PBS and incubated with 3% H_2O_2 in methanol for 10 min (25 °C). Cells were further washed with PBS and permeabilized using freshly prepared chilled Triton X-100 solution (0.1% v/v) and keeping on ice for 5 min. After washing twice with PBS, 50 mL of reaction mixture containing FLUOS-labelled dUTP and TdT were added and incubated at 37 °C for 1 h. The cells were finally washed, resuspended in PBS, put in the flow cytometer for data acquisition and analyzed using Deva software (Sheth et al., 2012).

2.8. Measurement of mitochondrial membrane potential ($\Delta\psi m$)

Mitochondrial membrane potential was determined as a measure of JC-1 dye retention (Molecular Probes Inc., Eugene). Briefly, JC-1 dye (1 μg/mL) was loaded in drug treated or untreated cells (5×10^4 per well), incubated for 30 min at 37 °C in a 5% CO_2 incubator and washed in PBS twice. Fluorescence was observed at 570 nm excitation/ 595 nm emission for the J-aggregate of JC1. $\Delta\psi m$ was determined as the ratio of the fluorescence of J-aggregate (aqueous phase) and monomer (membrane-bound) forms of JC1.

2.9. Caspase-3 assay

Firstly, the cells (5×10^4 per well) were seeded (200 μL culture medium) in a 96-well plate. After 16 h various doses of RLPLGA nanoparticles and RL were put into the wells to induce apoptosis. Caspase-3 activity was observed as per product manual (EMD Biosciences) using a fluorometer (Chen et al., 2010).

2.10. Intracellular reactive oxygen species (ROS) levels

For ROS levels determination, LNCaP cells (5×10^4 per well) were treated with RLPLGA nanoparticles and RL in 96-well plates. At 24 h, 5 μM of H_2DCFDA dye was loaded and incubated for 30 min. Fluorescence was measured at 488 nm excitation/515 nm emission wavelength using a fluorescence plate reader.

2.11. Cell cycle status

The seeded LNCaP cells (5×10^4 per well) were incubated with various concentrations of drugs and nanoparticles for 24 h and fixed in 70% ethanol. Subsequently, RNase A and propidium iodide were put to make a final concentration of 50 μg/mL each. The culture plate was then incubated at 4 °C for 60 min. The cells were observed using a FACS Calibur flow cytometer (BD Biosciences, San Jose, CA, USA) and cell cycle distribution was studied with Mod Fit LT software (Verity Software House, Topsham, ME, USA) (Horvath et al., 2007).

2.12. In vitro assessment of cytosatefy

MTT cell proliferation assay was used to evaluate *in vitro* cytotoxicity of RLPLGA nanoparticles and free RL on murine macrophages; RAW 264.7 (ATCC® TIB-71™). Briefly, flat-bottom 96 well plate was seeded with 5×10^4 per plate murine macrophages and incubated for 48 h at 37 °C in a CO_2 incubator. The cells were also exposed to RLPLGA nanoparticles and free RL at a wide range of concentrations (0–200 μM). The study was completed as per the method described in the Section 2.4 MTT assay.

2.13. Statistical analysis

All the *in vitro* experiments were performed in triplicate and standard error of the mean (SEM) was calculated. The statistical significance of differences between the groups was determined using ANOVA followed by Tukey's test by Graph Pad Prism 5 software and a *p*-value of < 0.05 was considered to be statistically significant.

3. Results

3.1. RP-HPLC method for resveratrol quantification

The concentration versus peak area calibration curve (ranging from 0.1 to 2 μg/mL) and representative peak (1 μg/mL) is shown in Fig. 1. The calibration data showed a linear curve with R^2 value of 0.9999. LOD and LOQ were determined to be 0.21 and 0.63 μg/mL. The same method was used for all *in vitro* studies.

3.2. Preparation of resveratrol-loaded nanoparticles

A total of 9 runs obtained from 2-factor 3-level factorial design was performed. Particle size and entrapment efficiencies for all the runs were determined (Table 1). The quadratic equation for both responses generated using Design Expert®8 software is presented as follows:

$$\text{Particle size (nm)} = 231.12 - 28.85\,\mathbf{A} - 33.53\,\mathbf{B} + 8.6\,\mathbf{AB} + 5.42\,\mathbf{A^2} + 59.77\,\mathbf{B^2}$$

$$\%EE = 86.18 + 7.15\,\mathbf{A} + 2.22\quad \mathbf{B} - 2.64\,\mathbf{AB} - 3.62\,A^2 - 19.56\,\mathbf{B^2}$$

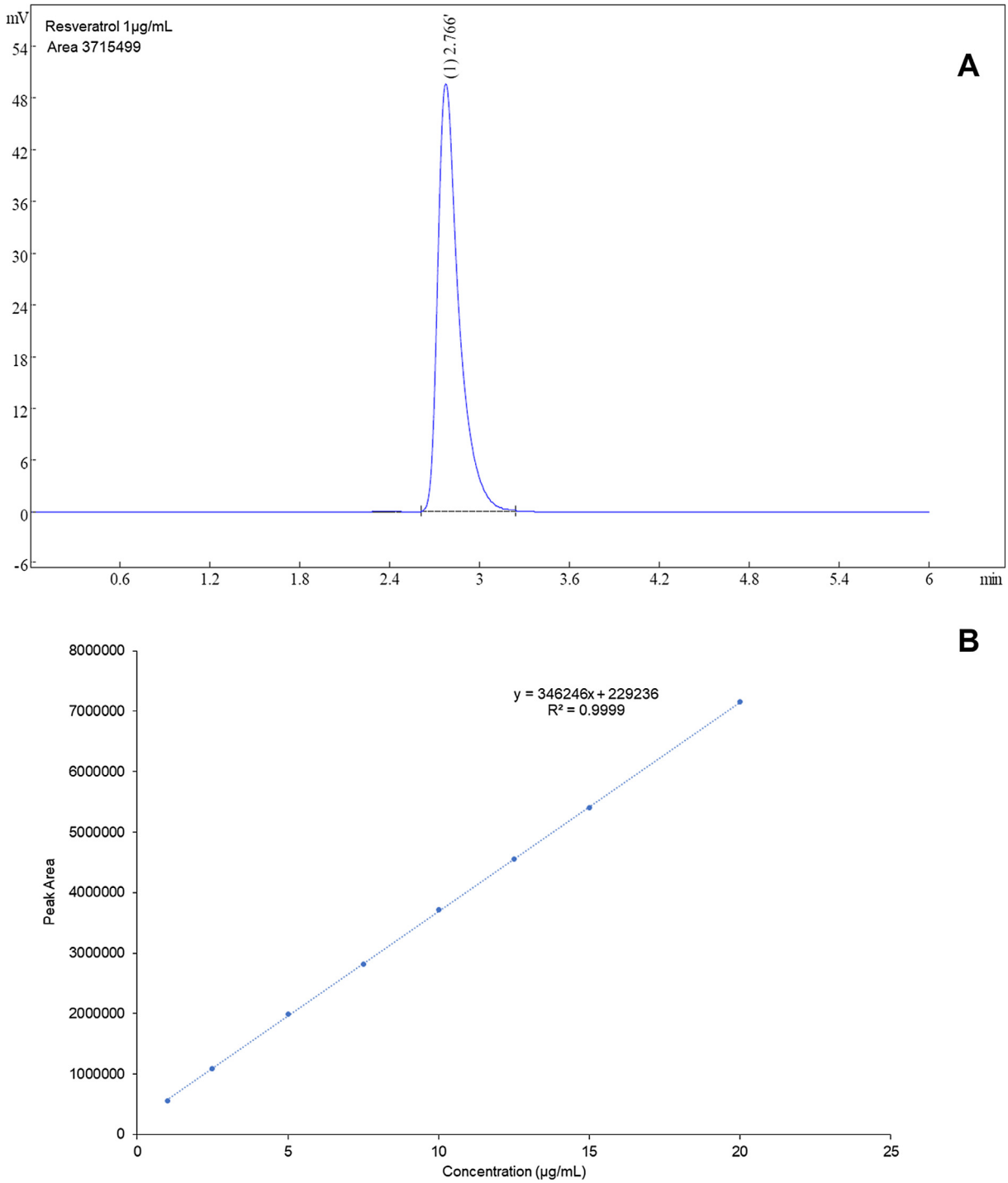

Fig. 1. Representative HPLC chromatogram and calibration curve for RL quantification.

The ANOVA performed on individual terms indicated that all the terms were significantly affecting the response ($p < 0.05$). Using the same software, numerical optimization was performed and a formula to obtain small particle size and high entrapment efficiency was derived. The software generated formula with maximum desirability was selected and prepared in the lab in triplicate. The particle size and %EE results showed an insignificant difference between the predicted and actual response (Table 2). This formula was considered to be optimized. Further characterization, anticancer properties, apoptosis, and safety study were performed using the same. 3D response surface and contour plots are shown in Fig. 2.

3.3. Characterization of nanoparticles

3.3.1. Particle size analysis

The average particle size and particle size distribution (polydispersity index) of RLPLGA nanoparticles was found to be 202.8 ± 2.64 nm and 0.17 ± 0.016 (Fig. 3A).

Table 1
3^2 - factorial design runs (n = 3).

Runs	Factor A PLGA/RL ratio	Factor B PVA Conc.	Response 1 Particle size (nm)	Response 2 %EE (%)
1	1:1	2.5	366.2 ± 7.25	50.28 ± 1.23
2	2:1	2.5	322.1 ± 8.22	65.98 ± 2.34
3	4:1	2.5	295.8 ± 6.57	69.71 ± 2.77
4	1:1	5	268.2 ± 8.17	75.59 ± 3.01
5	2:1	5	234.5 ± 9.55	85.54 ± 3.21
6	4:1	5	201.5 ± 2.66	90.18 ± 3.27
7	1:1	7.5	281.3 ± 3.65	61.25 ± 3.55
8	2:1	7.5	256.3 ± 6.59	67.91 ± 1.89
9	4:1	7.5	245.3 ± 5.87	70.12 ± 2.87

Table 2
The predicted and actual results for the optimized formula.

Formula	PLGA/RL ratio	PVA Conc. (mg/mL)	Particle size (nm)	%EE (%)
Predicted	4:1	5.21	206.029	89.541
Actual	4:1	5.21	202.8 ± 2.64	89.32 ± 3.51%

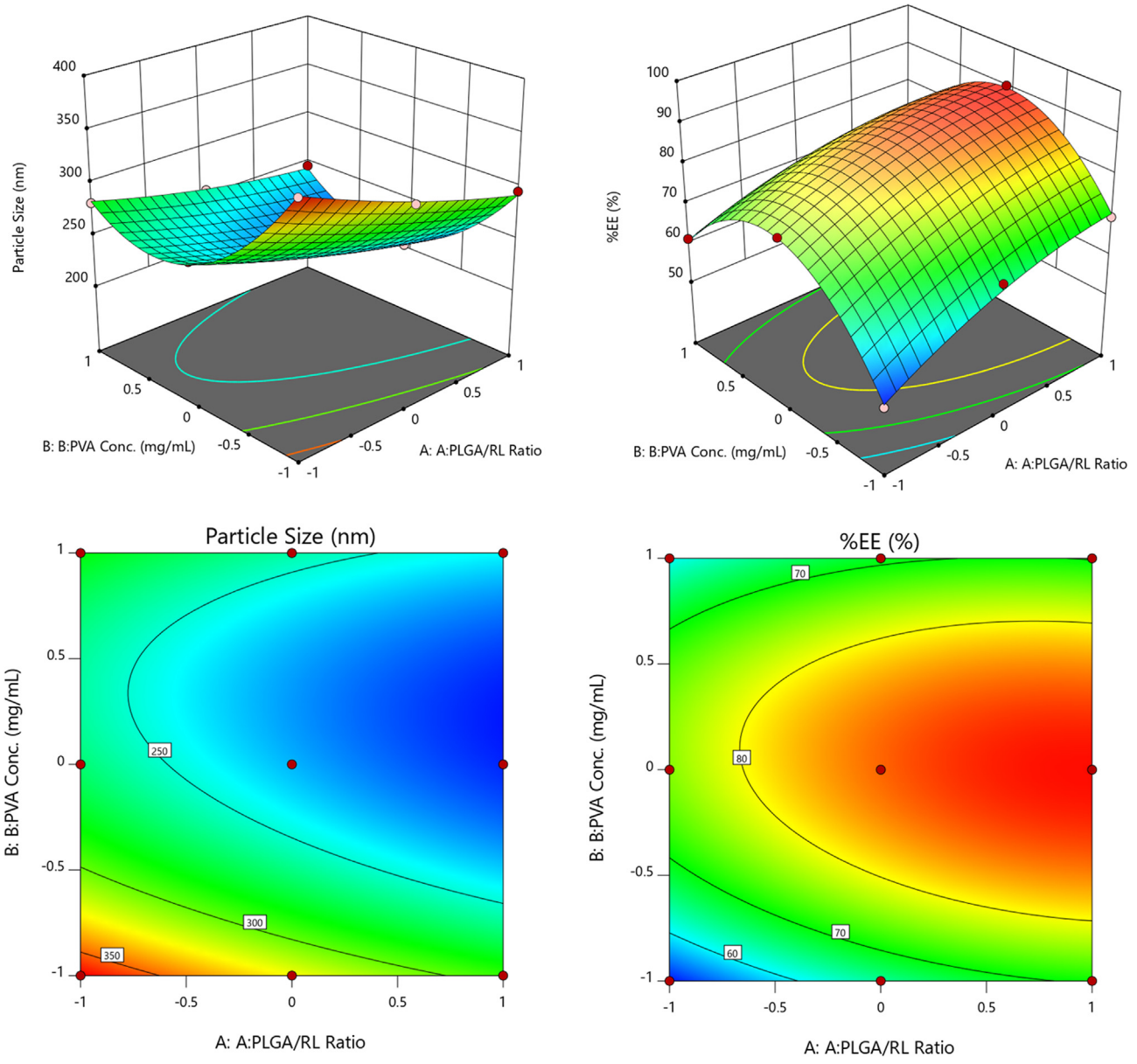

Fig. 2. 3D-response surface and contour plot showing the variation of response with respect to factors.

3.3.2. Transmission electron microscopy

TEM microphotograph showed nearly spherical particles (Fig. 3B). The average particle size was also determined by taking the size of 100 particles from all the four quadrants of a microscopic viewfinder (237.8 ± 4.93 nm). Both the measurements were found to be nearly similar to each other.

3.3.3. Entrapment efficiency

Entrapment efficiency of the optimized nanoparticle was 89.32 ± 3.51%.

3.3.4. Differential scanning calorimetry

Differential scanning calorimetry (DSC) thermogram showed a sharp peak of resveratrol while there was an absence of any sharp peak in the formulation which is an indication of complete entrapment of RL in PLGA. Both PLGA and nanoparticles showed a relatively broad peak between 45 and 55 °C (Fig. 3C).

3.3.5. In vitro drug release study

The drug release study showed a maximum release of 73.87 ± 3. 91% and 34.65 ± 2.34% with RLPLGA and RL after 24 h (Fig. 3D).

3.4. MTT assay

Significantly higher inhibition of LNCaP Cell Viability was observed with RLPLGA nanoparticles as compared to the plain drug at all concentrations (10–100 μM). Treatment revealed a dose-dependent reduction of LNCaP cells viability. IC_{50} and IC_{90} were observed to be 15.6 ± 1.49 and 41.1 ± 2.19 μM respectively. However, the IC_{50} (29.7 μM) and IC_{90} (77.2 μM) value by RL treatment were found to be nearly double as compared to RLPLGA nanoparticles (Fig. 4).

3.5. Analysis of phosphatidylserine (PS) externalization

Phospholipids translocation from the inner to the outer layer of the plasma membrane is a characteristic of the early phase of apoptosis in the cells. Ca^{2+} dependent phospholipid-binding protein, Annexin V has a high affinity for PS is generally used to show PS externalization. However, annexin V also labels necrotic cells. Thus, the cells were stained with propidium iodide (PI) to differentiate between the early apoptotic cells (annexin V +ve and PI −ve), late apoptotic cells (annexin V +ve and PI +ve), live cells (annexin V −ve and PI −ve) and necrotic cells (annexin V −ve and PI +ve). As shown in Fig. 4, a 65.60 ± 3.25% of RLPLGA nanoparticle treated LNCaP cells were stained positive for annexin V at 50 μM as compared to RL which showed only 39.79 ± 1.33% staining. The staining observed in both RL and RLPLGA were significantly higher as compared to control group (4.26 ± 0.52%) (Fig. 5).

3.6. TUNEL assay

Fragmentation of nuclear DNA into nucleosomal units is one of the prominent attributes of apoptotic cell death. In TUNEL assay, the proportion of DNA nicks can be calculated by determining the binding of dUTP– FLUOS to the nicked ends through TdT. The magnitude of fragmentation is directly proportional to the fluorescence obtained from dUTP–FLUOS. TUNEL assay revealed a significantly greater DNA nicking in LNCaP cells when treated with RLPLGA nanoparticles as compared to RL in a dose-dependent manner. The mean fluorescence intensity (MFI) of untreated LNCaP cells (796 ± 19.5) increased to 1269 ± 35.9, 2320 ± 56.2, and 3109 ± 116.1, 3976 ± 169.5 and 4738 ± 209.4 at lowest to the highest dose (10–50 μM), which was reasonably higher than RL (Fig. 6).

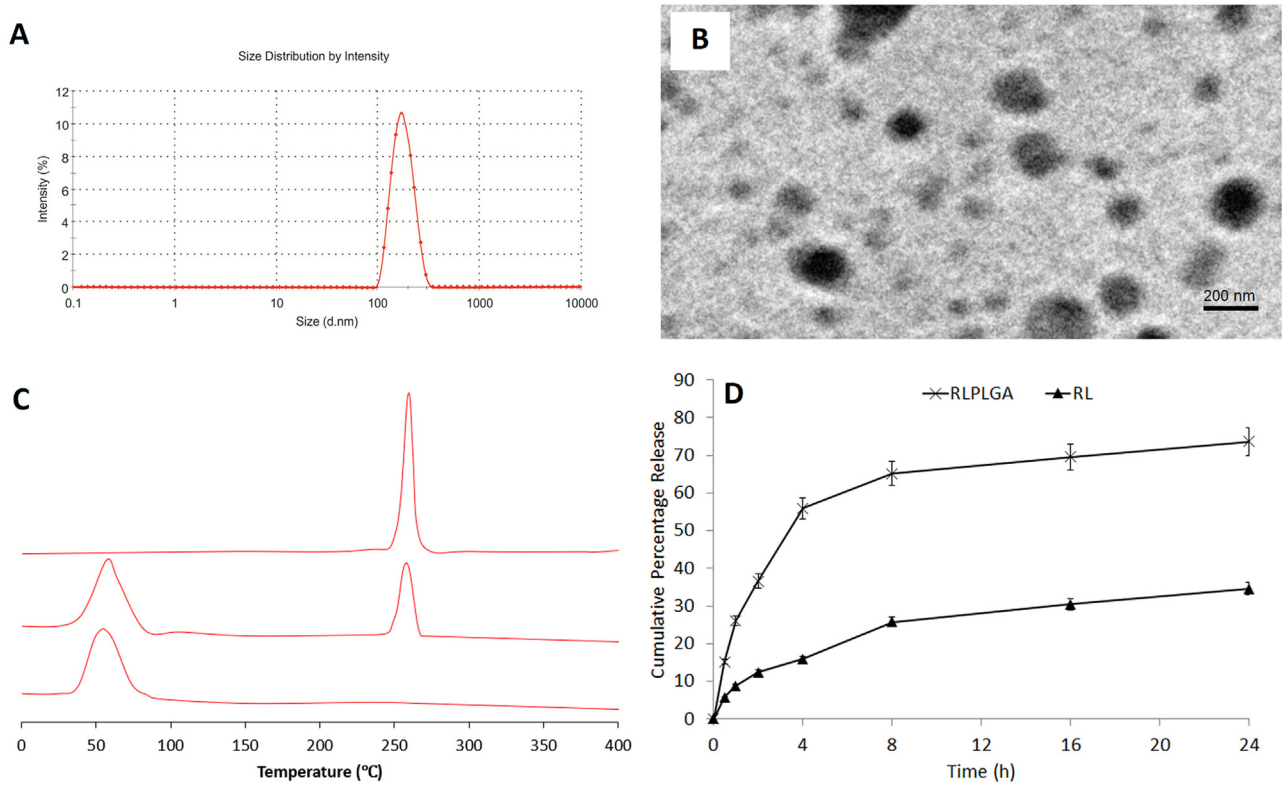

Fig. 3. Characterization of optimized nanoparticles (A) Particle size distribution, (B) TEM, (C) DSC and (D) Drug release profile.

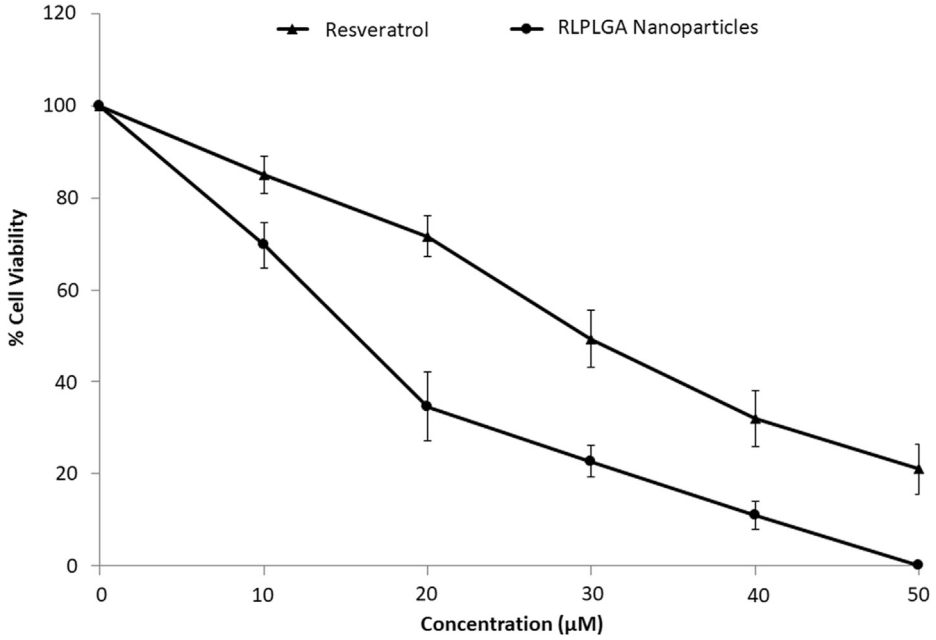

Fig. 4. The %cell viability vs concentration (μM) plot for RL and RLPLGA nanoparticles used to determine IC_{50} and IC_{90}.

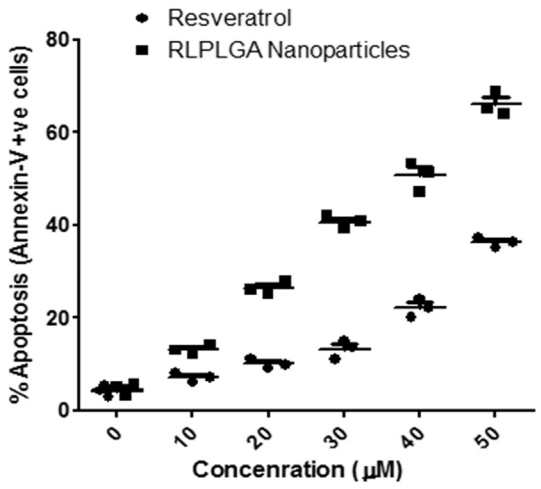

Fig. 5. Detection of apoptosis in LNCaP cells by annexin V-FITC and PI co-staining. Cells were treated with RLPLGA nanoparticles or resveratrol (0–50 μM) for 48 h and analyzed by flow cytometry. The graph represents the percentage of apoptotic cell population vs concentration (μM).

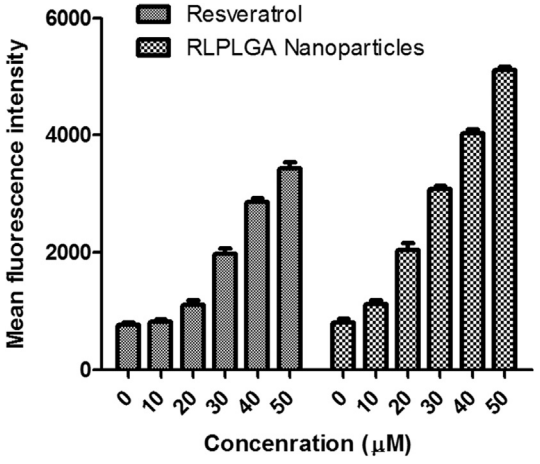

Fig. 6. RLPLGA nanoparticles treated LNCaP cells represent TdT-mediated dUTP nick-end labeling (TUNEL) positivity. LNCaP cells were incubated with RLPLGA nanoparticles or resveratrol (0–50 μM) for 48 h. Cells were fixed and stained with dUTP–FITC in the presence of TdT. Bar graphs representing MFI of TUNEL expression as analyzed by flow cytometry.

3.7. Measurement of mitochondrial membrane potential ($\Delta\psi m$)

Mitochondrial membrane potential (Δψm) was measured by using a lipophilic fluorescent cationic dye, JC-1 which freely permeates to the mitochondrial membrane and forms red fluorescent J-aggregates. The JC-1 stained viable cells show marked red fluorescence. However, an apoptotic stimulus brings a reduction in the Δψm which stops JC-1 to enter mitochondria. JC-1 remaining as cytosolic monomers emit a green fluorescence. Thus, the ratio of J-aggregates to monomers is a remarkable indicator of the mitochondrial membrane potential, which thereby allows distinguishing between apoptotic and non-apoptotic cells. In untreated LNCaP cells, the red/green fluorescence ratio was found to be 11.063 ± 2.364. The RLPLGA nanoparticles and RL treatment brought a significant decline in Δψm that consequentially led to a prevalence of JC-1 monomers with green fluorescence, and a reduction in the mean fluorescence intensity ratio to 0.755 ± 0.058 and 1.982 ± 0.152 at 50 μM, respectively (Fig. 7).

3.8. Caspase-3 assay

Caspase-3 mediates and its increased activation is a direct measure of both apoptosis and inflammation. It acts through aspartate-specific cleavage of many cellular substrates. Thus, the magnitude of caspase-3 activation was examined by kit based fluorogenic assay in LNCaP cells (Fig. 9). The caspase activity was found to be significantly higher in RLPLGA nanoparticles treated cells as compared to RL treatment at all doses in a dose-dependent manner.

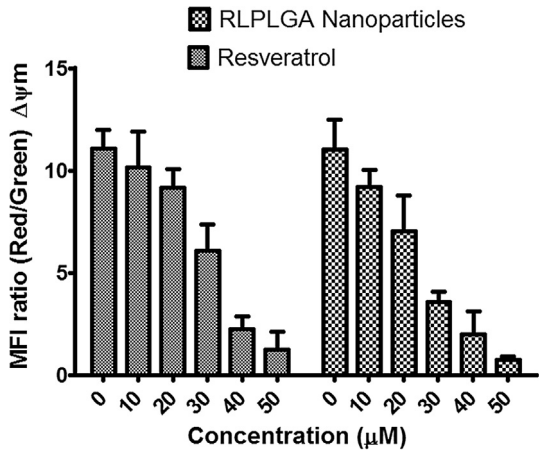

Fig. 7. The collapse of mitochondrial membrane potential in LNCaP cells by RLPLGA nanoparticles. LNCaP cells were incubated with RLPLGA nanoparticles and resveratrol (0–50 μM) for 48 h and probed with JC 1; bar diagram represents the ratio of red/green fluorescence intensity (ΔΨm).

3.9. Intracellular reactive oxygen species (ROS) levels

Intracellular ROS levels were determined using H_2DCFDA compound. H_2DCFDA is a lipophilic, membrane permeable compound which upon cleavage by intracellular esterases forms H_2DCF which is not able to transport outside the cells. H_2DCF, subsequently get oxidized by intracellular ROS to form a fluorescent DCF compound. Thus, the magnitude of green fluorescence is directly proportional to the amount of ROS generated. In LNCaP cells, RL and RLPLGA nanoparticles treatment enhanced ROS levels showing the significant increase in the green fluorescence at all concentrations as compared to the untreated LNCaP cells. Furthermore, RLPLGA showed significantly high ROS generation with respect to plain RL (Fig. 8).

3.10. Cell cycle status

LNCaP cells treatment with RLPLGA nanoparticles and RL was able to arrest the cell cycle at a G_1-S phase in a dose-dependent manner. At the concentration of 40 μM and 50 μM, RLPLGA nanoparticles and RL treatment showed no cells in G_2-M region, respectively (Table 3). However, the percentage of G_2-M region of untreated control cells was found to be nearly 30%.

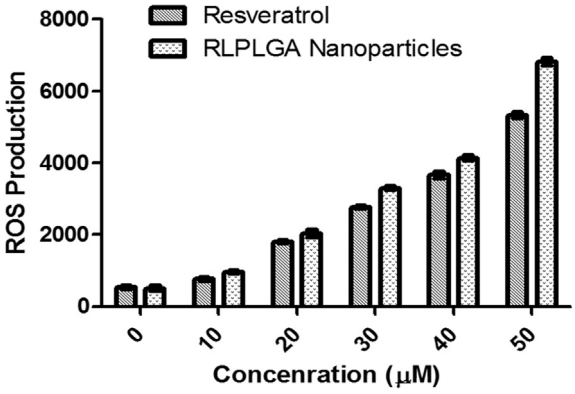

Fig. 8. Generation of ROS by RL and RLPLGA nanoparticles with respect to different concentrations in LNCaP cells.

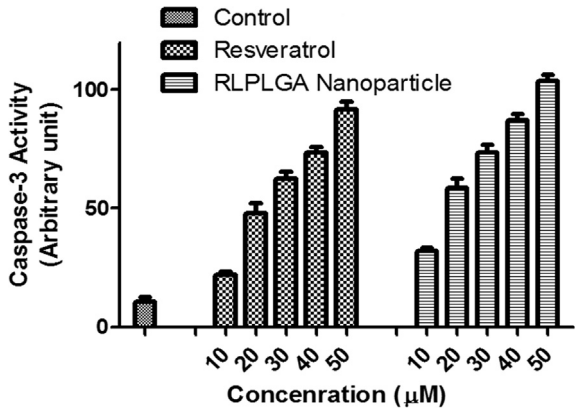

Fig. 9. Effects of different concentrations of RL and RLPLGA nanoparticles on caspase-3 activity within LNCaP cells.

Table 3
Flow cytometric analysis of the effect of RLPLGA Nanoparticles on LNCaP prostate cancer cell lines at 48 h.

Concentration (μM)	Resveratrol (RL)			RLPLGA		
	G_0-G_1	S	G_2-M	G_0-G_1	S	G_2-M
0	49.3%	22.1%	25.5%	48.6%	19.3%	30.9%
10	56.0%	19.9%	24.7%	58.8%	22.1%	19.0%
20	61.1%	20.6%	14.5%	69.7%	14.4%	11.2%
30	68.3%	26.0%	4.7%	71.2%	24.6%	3.1%
40	71.8%	24.0%	2.6%	79.1%	16.3%	0.0%
50	83.0%	16.2%	0.0%	90.4%	7.6%	0.0%

RLPLGA Nanoparticles arrested cells in G1-S phase transition in prostate cancer cells. LNCaP prostate cancer cell lines untreated and treated with (0–50 μM) RLPLGA Nanoparticles or Resveratrol for 48 h. The cells were then harvested, fixed in ethanol, stained with propidium iodide, and analyzed by FACS.

3.11. In vitro assessment of cytotosafety

Cytotoxicity study of RL and RLPLGA nanoparticles on murine macrophages [RAW 264.7 (ATCC® TIB-71™)] showed an interesting result as compared to LNCaP. As presented in Fig. 8, both RL and RLPLGA nanoparticles exhibited no adverse effect on the normal macrophages viability even at the concentration of 200 μM (Fig. 10).

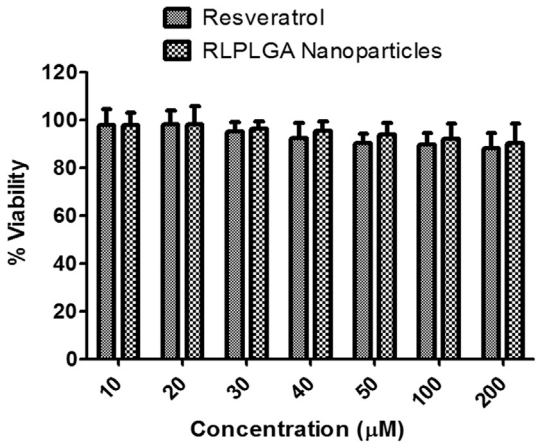

Fig. 10. Toxicity study of RL and RLPLGA nanoparticles on normal murine macrophages cell by MTT assay.

4. Discussion

Prostate cancer is one of the leading cause of mortality of men globally and is continued to be a growing concern in the past decade (Nelen, 2007). Even though most patients with localized prostate cancer is managed by surgery, there is a growing need to discover some effective adjuvant chemotherapeutic approaches in order to treat patients present with advanced prostate cancer disease or those who failed post-surgical interventions. Resveratrol is a phytoalexin produced naturally in several plant species like grapes, peanuts, and berries in response to fungal infection, mechanical injury or ultraviolet irradiation. Its cytostatic activity against the prostate cancer cells has been well demonstrated (Hsieh and Wu, 1999). In order to evaluate its potential against the LNCaP cells when encapsulated in a nanocarrier, we have developed a PLGA nanoparticle system. The formulation was optimized by 3^2-factorial design and characterized. From the quadratic equation generated for this experimental design, it was observed that for particle size there was a linear negative effect of both factors (A and B). This implies that the increase in each factor (PLGA/RL ratio and PVA conc.), individually contributes to lowering of particle size. At lower PLGA/RL ratio the more drug is available for encapsulation leading to an unorganized arrangement of matrix directing an increase in particle size. PVA is acting as a surfactant so its increase leads to rapid particle stabilization and lower particle size. Interestingly, intraction term AB as well as higher order terms A^2 and B^2 showed size increasing the effect. The effect of the simultaneous increase in PLGA and PVA concentration, as well as a quadratic increase in individual factors, might have lead to self-entanglement of the polymeric chain leading a higher particle size. The exactly reverse phenomenon was observed in case of %EE where linear increase in factors A and B showed increased %EE while the intraction and higher order terms have %EE decreasing effect. From this, we can conclude that, in this PLGA/RL/PVA nanoparticle system, a smaller sized particle is contributing to increased %EE, which might be due formation of a more stable matrix and lower leach out of drug from the system. Also, %EE tells the amount of drug that actually gets into the particles with respect to the amount added. So, a smaller particle size means a higher available surface to volume ratio and there could be an increased adhesion of RL molecule over the surface of the particles.

A series of comparative *in vitro* studies encompassing MTT assay and levels various apoptotic markers were performed to analyze the effect of RLPLGA nanoparticles with respect to RL. A clear evidence for enhanced LNCaP growth inhibition was observed for RLPLGA nanoparticles, which exhibited an IC_{50} of 15.6 μM and IC_{90} of 41.1 μM as compared to RL with having nearly double IC_{50} and IC_{90}. There are three possible reasons for increased efficacy of RLPLGA: (I) selective endocytosis of PLGA nanoparticles, (II) enhanced drug release and (III) Efflux transport inhibition by PLGA. The selective endocytosis of PLGA nanoparticles in LNCaP cells has been reported by Dhar et al. (2008). Moreover, the effect of enhanced drug release from nanoparticle could be another reason as we have used RL as well as RLPLGA suspended in water for the MTT assay. The greater drug concentration around the cells might have led to increased transport into the cells. However, RL transport from plain drug or from RLPLGA nanoparticles might be effluxed out of the cells by p-glycoproteins. But when RL is transported through nanoparticles, the PLGA is capable of inhibiting such efflux as mentioned previously (Xu et al., 2014). So, the major mechanism of enhancement of the activity by RLPLGA can be attributed to the selective internalization of nanoparticles in combination with blockade of efflux transport by PLGA.

Permeabilization of mitochondrial membranes can cause cell death either by apoptosis or necrosis. A decrease in mitochondrial membrane potential ($\Delta\psi m$) is commonly attributed to an early transformation leading to apoptosis. The reduction of $\Delta\psi m$ after inner mitochondrial membrane permeabilization activates the release of numerous apoptotic factors. RL has been studied to show anticancer activity against many prostate cancer cell lines which and reported causing a decrease in $\Delta\psi m$ (Kumar et al., 2017). Like RL, the PLGA encapsulated counterpart, RLPLGA nanoparticles also caused mitochondrial membrane depolarization and in a significantly greater magnitude. Mitochondria are the main cellular organelle which produces ROS during normal cellular metabolism. Many antioxidant enzymes present in the cytosol like superoxide dismutase (SOD) and catalase (CAT) offer cellular defense against oxidative stress-induced cell damage (Michaeloudes et al., 2011). Our study revealed that RLPLGA nanoparticles (as well as RL, up to a lesser extent) were able to induce apoptosis in LNCaP cells mainly by mitochondrial-dependent pathway (manifested by a significant drop in mitochondrial membrane potential) and generation of reactive oxygen species (ROS). However, expression of some cellular antioxidants enzymes is hindered during this condition, leading to disturbance in redox homeostasis that follows up with apoptosis (Baluchamy et al., 2012; Kim et al., 2011). RL is known to an induced generation of ROS prostate cancer cells and causing ROS mediated apoptosis (Chen et al., 2010). This effect was more pronounced with RL loaded PLGA nanoparticles used in our study. Some previous studies also support this outcome by producing evidence for RL as an anti-cancer agent and theoretical molecular targets (Shimizu et al., 2006). For example, RL at a concentrations range of 25–100 μM has exhibited to induce chondrosarcoma cell apoptosis (Chao et al., 2017).

Moreover, caspase-3 activation is measured to be the sign of final commitment to cell death and a hallmark of apoptosis. RLPLGA nanoparticles induced the increase in caspase-3 activity in LNCaP cells to a greater extent than RL substantiating the anticancer activity of resveratrol against prostate cancer.

During programmed cell death (PCD), phosphatidylserine (PS) is externalized towards the outer surface of the plasma membrane (Chen et al., 2017). RL and RLPLGA nanoparticles treated LNCaP cells also demonstrated enhanced PS exposures which were significantly higher than RL treatment evidenced by the increased annexin V binding. The alterations in the nuclear material during PCD were observed and *in situ* TUNEL of nicked DNA was clearly detected with RLPLGA nanoparticles which is a strong evidence of apoptosis in LNCaP cells. Similar results were also observed with RL against PC-3M-MM2 cells (Sheth et al., 2012). There was a remarkable activity of RL and RLPLGA nanoparticles in terms of cell cycle arrest. The reductions in cell count were also found to be linked to cell cycle arrest at G_1-S transition phase (Chen et al., 2010; Sheth et al., 2012). Lastly, when RL and RLPLGA were exposed to normal peritoneal macrophages, there was no evidence of toxicity even at a dose level of 200 μM, clearly demonstrating the safe nature of RL and RLPLGA towards normal cells.

5. Conclusion

In this study, the feasibility of resveratrol loaded PLGA nanoparticles to inhibit the LNCaP cell growth has been studied and compared with plain resveratrol. Through MTT cytotoxicity assay and combined use of different apoptotic markers such as PS externalization, TUNEL assay, analysis of mitochondrial membrane potential, cell cycle status, caspase-3 assay and assessment of ROS generation, we have established that RLPLGA nanoparticles induced apoptosis in LNCaP with no adverse effect on normal macrophages cells. Our study broadens the scope for future designing and establishment of the nanotechnology-based chemotherapeutic strategies for improved management of prostate cancer.

Acknowledgment

This work was financially supported by Deanship of Scientific Research (DSR), Grant No. 43509010. Authors would like to acknowledge Faculty of Medicine, Umm Al-Qura University, Makkah (Ministry of Education) for providing the facility for research.

Conflict of interest

Authors declare no conflict of interests.

References

Ahmad, I., Anwar, M., Akhter, S., Thakur, P., Chawla, R., Sharma, R.K., Ali, A., Ahmad, F.J., 2016. Supercritical fluid technology-based trans-resveratrol sln for long circulation and improved radioprotection. J. Pharm. Innovation 11 (4), 308–322.

Anuchapreeda, S., Fukumori, Y., Okonogi, S., Ichikawa, H., 2011. Preparation of lipid nanoemulsions incorporating curcumin for cancer therapy. J. Nanotechnol. 2012.

Baluchamy, S., Ravichandran, P., Ramesh, V., He, Z., Zhang, Y., Hall, J.C., Jejelowo, O., Gridley, D., Wu, H., Ramesh, G.T., 2012. Reactive oxygen species mediated tissue damage in high energy proton irradiated mouse brain. Mol. Cell. Biochem. 360 (1–2), 189–195.

Chao, S.C., Chen, Y.J., Huang, K.H., Kuo, K.L., Yang, T.H., Huang, K.Y., Wang, C.-C., Tang, C.-H., Yang, R.-S., Liu, S.H., 2017. Induction of sirtuin-1 signaling by resveratrol induces human chondrosarcoma cell apoptosis and exhibits antitumor activity. Sci. Rep. 7 (1), 3180. https://doi.org/10.1038/s41598-017-03635-7.

Chen, Q., Ganapathy, S., Singh, K.P., Shankar, S., Srivastava, R.K., 2010. Resveratrol induces growth arrest and apoptosis through activation of FOXO transcription factors in prostate cancer cells. PLoS One 5 (12), e15288. https://doi.org/10.1371/journal.pone.0015288.

Chen, X., Xiao, W., Chen, W., Liu, X., Wu, M., Bo, Q., ... Liu, Y., 2017. MicroRNA-26a and -26b inhibit lens fibrosis and cataract by negatively regulating Jagged-1/Notch signaling pathway. Cell Death Differ. 24 (11), 1990. https://doi.org/10.1038/cdd.2017.147.

Cvetković, Ž.S., Nikolić, V.D., Savić, I.M., Savić-Gajić, I.M., Nikolić, L.B., 2015. Development and validation of an RP-HPLC method for quantification of trans-resveratrol in the plant extracts. Hemijska industrija 69 (6), 679.

Dhar, S., Gu, F.X., Langer, R., Farokhzad, O.C., Lippard, S.J., 2008. Targeted delivery of cisplatin to prostate cancer cells by aptamer functionalized Pt(IV) prodrug-PLGA-PEG nanoparticles. Proc. Natl. Acad. Sci. U. S. A. 105 (45), 17356–17361. https://doi.org/10.1073/pnas.0809154105.

Ding, X.-Z., Adrian, T.E., 2002. Resveratrol inhibits proliferation and induces apoptosis in human pancreatic cancer cells. Pancreas 25 (4), e71–e76.

Guo, L., Peng, Y., Yao, J., Sui, L., Gu, A., Wang, J., 2010. Anticancer activity and molecular mechanism of resveratrol-bovine serum albumin nanoparticles on subcutaneously implanted human primary ovarian carcinoma cells in nude mice. Cancer Biotherapy Radiopharm. 25 (4), 471–477.

Horvath, Z., Marihart-Fazekas, S., Saiko, P., Grusch, M., Oezsuey, M., Harik, M., ... Fritzer-Szekeres, M., 2007. Novel resveratrol derivatives induce apoptosis and cause cell cycle arrest in prostate cancer cell lines. Anticancer Res. 27 (5A), 3459–3464.

Hsieh, T.-C., Wu, J.M., 1999. Differential effects on growth, cell cycle arrest, and induction of apoptosis by resveratrol in human prostate cancer cell lines. Exp. Cell Res. 249 (1), 109–115.

Jabir, N.R., Tabrez, S., Ashraf, G.M., Shakil, S., Damanhouri, G.A., Kamal, M.A., 2012. Nanotechnology-based approaches in anticancer research. Int. J. Nanomed. 7, 4391.

Johannsen, M., Thiesen, B., Wust, P., Jordan, A., 2010. Magnetic nanoparticle hyperthermia for prostate cancer. Int. J. Hyperth. 26 (8), 790–795.

Kim, D., Jeong, Y.Y., Jon, S., 2010. A drug-loaded aptamer– gold nanoparticle bioconjugate for combined CT imaging and therapy of prostate cancer. ACS Nano 4 (7), 3689–3696.

Kim, S.-J., Jung, H.-J., Lim, C.-J., 2011. Disruption of redox homeostasis and induction of apoptosis by suppression of glutathione synthetase expression in a mammalian cell line. Free Radical Res. 45 (9), 1040–1051.

Kjær, T.N., Ornstrup, M.J., Poulsen, M.M., Jørgensen, J.O.L., Hougaard, D.M., Cohen, A. S., ... Pedersen, S.B., 2015. Resveratrol reduces the levels of circulating androgen precursors but has no effect on, testosterone, dihydrotestosterone, PSA levels or prostate volume. A 4-month randomised trial in middle-aged men. Prostate 75 (12), 1255–1263.

Kumar, S., Eroglu, E., Stokes 3rd, J.A., Scissum-Gunn, K., Saldanha, S.N., Singh, U.P., ... Mishra, M.K., 2017. Resveratrol induces mitochondria-mediated, caspase-independent apoptosis in murine prostate cancer cells. Oncotarget 8 (13), 20895–20908. https://doi.org/10.18632/oncotarget.14947.

Michaeloudes, C., Sukkar, M.B., Khorasani, N.M., Bhavsar, P.K., Chung, K.F., 2011. TGF-β regulates Nox4, MnSOD and catalase expression, and IL-6 release in airway smooth muscle cells. Am. J. Physiol.-Lung Cell. Mol. Physiol. 300 (2), L295–L304.

Narayanan, N.K., Nargi, D., Randolph, C., Narayanan, B.A., 2009. Liposome encapsulation of curcumin and resveratrol in combination reduces prostate cancer incidence in PTEN knockout mice. Int. J. Cancer 125 (1), 1–8.

Nelen, V., 2007. Epidemiology of Prostate Cancer Prostate Cancer. Springer, pp. 1–8.

Paller, C.J., Rudek, M.A., Zhou, X.C., Wagner, W.D., Hudson, T.S., Anders, N., ... Antonarakis, E.S., 2015. A phase I study of muscadine grape skin extract in men with biochemically recurrent prostate cancer: Safety, tolerability, and dose determination. Prostate 75 (14), 1518–1525.

Patel, K.R., Brown, V.A., Jones, D.J., Britton, R.G., Hemingway, D., Miller, A.S., ... Crowell, J.A., 2010. Clinical pharmacology of resveratrol and its metabolites in colorectal cancer patients. Cancer Res. 70 (19), 7392–7399.

Pozo-Guisado, E., Alvarez-Barrientos, A., Mulero-Navarro, S., Santiago-Josefat, B., Fernandez-Salguero, P.M., 2002. The antiproliferative activity of resveratrol results in apoptosis in MCF-7 but not in MDA-MB-231 human breast cancer cells: cell-specific alteration of the cell cycle. Biochem. Pharmacol. 64 (9), 1375–1386.

Ratan, H.L., Steward, W.P., Gescher, A.J., Mellon, J.K., 2002. Resveratrol—a prostate cancer chemopreventive agent? Paper presented at the Urologic Oncology: Seminars and Original Investigations.

Richard, T., Pawlus, A.D., Iglésias, M.L., Pedrot, E., Waffo-Teguo, P., Mérillon, J.M., Monti, J.P., 2011. Neuroprotective properties of resveratrol and derivatives. Ann. N. Y. Acad. Sci. 1215 (1), 103–108.

Sanna, V., Sechi, M., 2012. Nanoparticle therapeutics for prostate cancer treatment. Maturitas 73 (1), 27–32.

Seeni, A., Takahashi, S., Takeshita, K., Tang, M., Sugiura, S., Sato, S., Shirai, T., 2008. Suppression of prostate cancer growth by resveratrol in the transgenic rat for adenocarcinoma of prostate (TRAP) model. Asian Pac. J. Cancer Prev. 9 (1), 7–14.

She, Q.-B., Bode, A.M., Ma, W.-Y., Chen, N.-Y., Dong, Z., 2001. Resveratrol-induced activation of p53 and apoptosis is mediated by extracellular-signal-regulated protein kinases and p38 kinase. Cancer Res. 61 (4), 1604–1610.

Sheth, S., Jajoo, S., Kaur, T., Mukherjea, D., Sheehan, K., Rybak, L.P., Ramkumar, V., 2012. Resveratrol reduces prostate cancer growth and metastasis by inhibiting the Akt/MicroRNA-21 pathway. PLoS One 7 (12), e51655. https://doi.org/10.1371/journal.pone.0051655.

Shih, A., Zhang, S., Cao, H.J., Boswell, S., Wu, Y.-H., Tang, H.-Y., ... Lin, H.-Y., 2004. Inhibitory effect of epidermal growth factor on resveratrol-induced apoptosis in prostate cancer cells is mediated by protein kinase C-α. Mol. Cancer Ther. 3 (11), 1355–1364.

Shimizu, T., Nakazato, T., Xian, M.J., Sagawa, M., Ikeda, Y., Kizaki, M., 2006. Resveratrol induces apoptosis of human malignant B cells by activation of caspase-3 and p38 MAP kinase pathways. Biochem. Pharmacol. 71 (6), 742–750.

Singh, A., Ahmad, I., Ahmad, S., Iqbal, Z., Ahmad, F.J., 2016. A novel monolithic controlled delivery system of resveratrol for enhanced hepatoprotection: nanoformulation development, pharmacokinetics and pharmacodynamics. Drug Dev. Ind. Pharm. 42 (9), 1524–1536.

Singh, A., Ahmad, I., Akhter, S., Jain, G.K., Iqbal, Z., Talegaonkar, S., Ahmad, F.J., 2013. Nanocarrier based formulation of Thymoquinone improves oral delivery: stability assessment, in vitro and in vivo studies. Colloids Surf. BBiointerfaces 102, 822–832.

Walle, T., Hsieh, F., DeLegge, M.H., Oatis, J.E., Walle, U.K., 2004. High absorption but very low bioavailability of oral resveratrol in humans. Drug Metab. Dispos. 32 (12), 1377–1382.

Wang, T.T., Hudson, T.S., Wang, T.-C., Remsberg, C.M., Davies, N.M., Takahashi, Y., ... Perkins, S.N., 2008. Differential effects of resveratrol on androgen-responsive LNCaP human prostate cancer cells in vitro and in vivo. Carcinogenesis 29 (10), 2001–2010.

Xu, L., Li, H., Wang, Y., Dong, F., Wang, H., Zhang, S., 2014. Enhanced activity of doxorubicin in drug resistant A549 tumor cells by encapsulation of P-glycoprotein inhibitor in PLGA-based nanovectors. Oncol. Lett. 7 (2), 387–392.

Zhu, W., Qin, W., Zhang, K., Rottinghaus, G.E., Chen, Y.-C., Kliethermes, B., Sauter, E. R., 2012. Trans-resveratrol alters mammary promoter hypermethylation in women at increased risk for breast cancer. Nutr. Cancer 64 (3), 393–400.